Computational study of effects of uniaxial compression during processes of spinodal decomposition

Mikihito Takenaka and Takeji Hashimoto*
Department of Polymer Chemistry, Faculty of Engineering, Kyoto University, Kyoto 606, Japan

Toshihiro Kawakatsu
Department of Physics, Tokyo Metropolitan University, Hachioji, Tokyo 192-03, Japan

Kyozi Kawasaki
Fakultät für Physik, Universität Konstanz, Postfach 55 60, D-78434 Konstanz, Germany
(Received 3 January 1995)

We present a computational study on the effects of a uniaxial compression with compression ratio $\frac{1}{2}$ on the ordering processes via spinodal decomposition (SD), by numerically integrating the time-dependent Ginzburg-Landau equation. We investigate the pattern growth and two-dimensional structure factors both after a compression in the intermediate stage SD and after a compression in the late stage SD. The results indicate that the compression in the intermediate stage SD causes the phase-separated structure to orient with its interfaces in the direction parallel to the compression axis, and that the compression in the late stage SD causes the phase-separated structure to orient with its interfaces in the direction perpendicular to the compression axis.

PACS number(s): 64.60.Cn, 64.70.Ja, 83.80.Es, 47.11.+j

I. INTRODUCTION

The dynamics of phase separation via spinodal decomposition (SD) of binary mixtures has been one of the active research topics of nonequilibrium statistical physics, and isothermal processes of SD have been studied for various kinds of binary mixtures [1]. Recently, the effects of external fields, e.g., stress or flow fields, on the phase separation via SD have attracted much attention from both theoretical [2] and experimental [3] viewpoints. The processes of the phase separation via SD is a nonlinear phenomenon and hence dynamical evolution of the phase-separated structure depends on the paths that the systems take before the execution of the process under consideration. We may anticipate that a unique path involving an application of an external field forms a unique phase-separated structure that is not obtained by an isothermal process without external fields.

Hashimoto, Izumitani, and Takenaka [4] reported the homogenization process of an immiscible mixture of poly(styrene-*ran*-butadiene) (SBR) and polybutadiene (PB) (designated hereafter SBR-PB) by Baker's transformation. In Baker's transformation, the film specimens of the mixtures are subjected to repeated unaxial compression. They found that the phase-separated mixture was brought into the single-phase region near the critical point by the transformation. The proposed mechanism of homogenization by the transformation is as follows. The wavelength of concentration fluctuations parallel to the compression axis was compressed by the transformation so that the concentration fluctuations along this axis become unstable, resulting in the dissolution of the concentration fluctuations.

Hashimoto and Izumitani [5] further extended their studies to investigate the effects of uniaxial compression on the kinetics of isothermal SD processes of the SBR-PB mixture of 60 °C. They applied uniaxial compression for the film specimens of the mixture at a particular stage of SD and investigated the kinetics and ordering processes after compression. Figure 1 shows an example of such

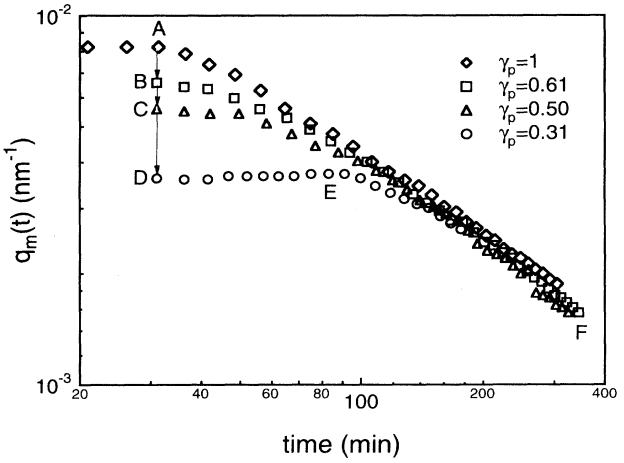

FIG. 1. Time change in peak position $q_m(t)$ of the scattering function during the SD processes of SBR-PB. Uniaxial compression of various compression ratios was imposed on the mixture during SD, 31 min after phase separation at 60 °C. $\gamma_p = l/l_0$ are equal to 1 (diamonds), 0.608 (squares), 0.504 (triangles), and 0.310 (circles), where l_0 and l are the thickness of the samples before and after uniaxial compression, respectively.

*Author to whom correspondence should be addressed.

studies in which the uniaxial compression of various compression ratios $\gamma_p \equiv l/l_0$ (l_0 and l, respectively, being the thicknesses of the sample parallel to the compression axis before and after the compression) was applied 31 min after onset of phase separation, which corresponds to an end of the early stage SD of this system [6]. They observed the time change in the scattered intensity as a function of the magnitude of the scattering vector $\mathbf{q}$ in the direction perpendicular to the compression direction (q_x or q_y directions in Fig. 2) before and after compression by the time-resolved light scattering method. Here $q \equiv |\mathbf{q}|$ is defined by

$$q = (4\pi/\lambda)\sin(\theta/2) , \quad (1)$$

with λ and θ being the wavelengths of the incident beam and the scattering angle in the medium, respectively.

If compression occurs according to an isochronal affine deformation, the width of the specimen in the directions perpendicular to the compression direction becomes $1/\sqrt{\gamma_p}$ times as wide as the original width. Correspondingly, the wavelength of a particular Fourier mode of the concentration fluctuations in this direction is also elongated by a factor of $1/\sqrt{\gamma_p}$ (see Fig. 2). The rate of compression used in their studies is much faster than the growth rate for the dominant mode of the concentration fluctuations [7], so that the domain growth does not effectively occur during the compression process. However, this rate is much slower than the molecular relaxation rate, so that the compression does not involve molecular orientation and deformations [6]. The flow induced by the compression gives rise to deformation of the phase-separated structure in which molecules are essentially relaxed, unoriented and undeformed. Since the system is still thermodynamically unstable, the domains grow further, even after the application of the compression, under an initial constraint given by this deformation.

In Fig. 1, a time evolution of the wave number $q_m(t)$ at the peak position of the scattered intensity during the SD processes of SBR-PB is plotted as a function of time t after onset of phase separation and at 60 °C. The results obtained in their study are as follows: before compression and at 31 min after the onset of SD, the time evolution of scattered intensity at various q is approximated by Cahn's linearized theory [8], i.e., the scattered intensity at a given q grows exponentially with time and the peak scattered intensity appears at q defined as $q_m(0) \cong 8 \times 10^{-3}$ nm^{-1}. In this time domain the spatially periodic concentration fluctuation grows in the mixture in such a way that the wavelength of the dominant Fourier mode of the fluctuations is essentially kept constant with t, equal to $2\pi/q_m(0)$. By applying compression, the original peak position $q_m(0)$ of the scattered intensity [see pattern (2) in Fig. 2] shifts to $q_m(0)\sqrt{\gamma_p}$ in

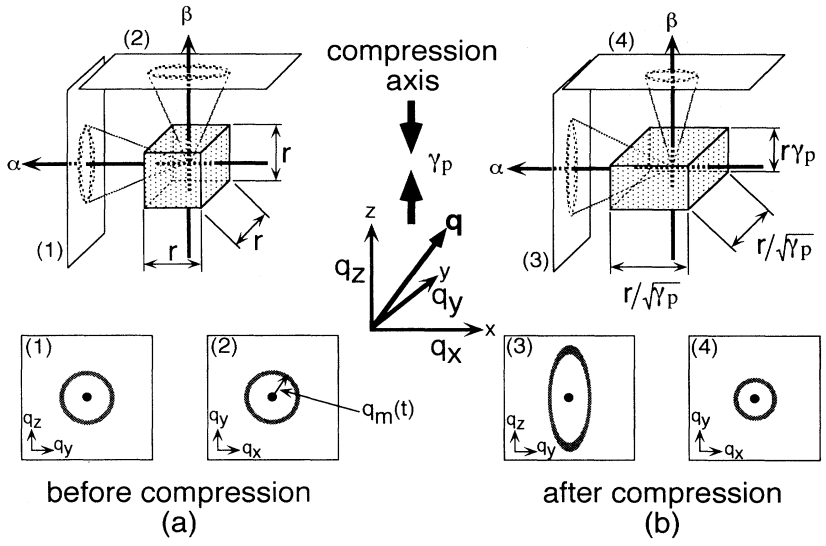

FIG. 2. Schematic illustration of the optical geometry and the change in the scattering pattern caused by uniaxial compression of the compression ratio γ_p. Thick arrows marked α and β are the propagation directions of incident beams. x and y axes are defined as the directions perpendicular to the compression axis and the z axis is defined as the direction parallel to the compression axis. q_x and q_y are components of wave vector $\mathbf{q}$ in the direction perpendicular to the compression axis and q_z is one parallel to the compression axis. By using beams α and β, respectively, the scattering patterns in the $q_y q_z$ plane and in the $q_x q_y$ plane are obtained. Before compression (a), the scattering pattern is isotropic as shown in patterns (1) and (2), since the structure is isotropic. After the compression (b), the structure is elongated to the q_x and q_y directions by a factor of $1/\sqrt{\gamma_p}$ so that the scattering pattern in the q_x, q_y plane shrinks by a factor of $\sqrt{\gamma_p}$, as shown in pattern (4). On the other hand, the scattering pattern in the $q_y q_z$ plane is elongated along the q_z direction by a factor of $1/\gamma_p$ and shrinks along the q_y direction by a factor of $\sqrt{\gamma_p}$, as shown in pattern (3), since the structure is compressed along the compression axis.

the $q_x q_y$ plane [see pattern (4) in Fig. 2] or, as seen in the change of $q_m(t)$, from point A to B, C, or D in Fig. 1. After compression, the peak position $q_m(t)$ keeps constant for some time in the curve DE for $\gamma_p = 0.31$ in Fig. 1. Then the peak wave number starts to decrease with time as seen in the curve EF in Fig. 1, in the same manner as that for the undeformed specimen. The time domain where the peak position stays constant becomes longer with decreasing compression ratio γ_p. While the peak position stays constant, the scattering intensity grows exponentially with time [5].

In this paper we study the effects of uniaxial compression on SD processes, especially on the dynamics and phase-separated structure, with computer simulation. In the simulation, we can study without difficulty the phase-separated structure in the $q_z q_y$ plane parallel to the compression axis, the study of which is difficult in experiment and has not actually been carried out in the experiments. Thus, we can anticipate obtaining important information which is difficult to obtain in experiments.

II. SIMULATION METHOD

We used the time-dependent Ginzburg-Landau (TDGL) equation [9] to study the dynamics of SD processes in A-B binary mixtures, where a binary mixture is represented by a continuous field. If we define the order parameter field as $\psi(\mathbf{r},t) \equiv \rho_A(\mathbf{r},t) - \rho_B(\mathbf{r},t)$, where $\rho_A(\mathbf{r},t)$ and $\rho_B(\mathbf{r},t)$ are the densities of A and B components, respectively, at position $\mathbf{r}$ and at time t, the time evolution of the order parameter $\psi(\mathbf{r},t)$ is expressed as

$$\frac{\partial \psi(\mathbf{r},t)}{\partial t} = L\nabla^2[-D\nabla^2\psi(\mathbf{r},t) - c\psi(\mathbf{r},t) + u\{\psi(\mathbf{r},t)\}^3] , \tag{2}$$

where L is the transport coefficient, and c, u, and D are positive constants. It should be noted that the thermal noise effects [10] and the hydrodynamics interaction effects [11] are neglected in Eq. (2). Adjusting the units of time, length, and the order parameter, we can set $L=1$, $c=1$, $u=1$, and $D=1$ without loss of generality. The parameters L, c, and D are related to those that characterize the early stage SD, predicted on the basis of the following linearized time evolution equation. Namely, if we neglect the $\{\psi(\mathbf{r},t)\}^3$ term, we find the following linearized equation for the q-Fourier components $\psi_q(t)$ of $\psi(\mathbf{r},t)$:

$$\frac{\partial \psi_q(t)}{\partial t} = Lq^2[c - Dq^2]\psi_q(t) . \tag{3}$$

This equation is valid only in the early stage SD, where the magnitude of $\psi(\mathbf{r},t)$ is small. Rearranging Eq. (3), we obtain the following equation:

$$\frac{\partial \psi_q(t)}{\partial t} = D_{\text{app}} q^2 \left[1 - \frac{q^2}{2q_m(0)^2}\right] \psi_q(t) , \tag{4}$$

where D_{app}, the mutual diffusion coefficient [6], is given by

$$D_{\text{app}} = Lc \tag{5}$$

and $q_m(0)$ is the dominant mode of $\psi(\mathbf{r},t)$ which grows with a maximum growth rate

$$q_m(0) = \left[\frac{c}{2D}\right]^{1/2} . \tag{6}$$

D_{app} and $q_m(0)$ become 1 and $1/\sqrt{2}$, respectively, by using $L=1$, $c=1$, and $D=1$ in this study.

Our simulation was carried out in two-dimensional (2D) space. In order to study computationally the time evolution of ψ, we divided the two-dimensional space into small cells whose size $\Delta r = 1$ and numerically integrated Eq. (2) in the discrete space up to $t=1000$ with a time step $\Delta t = 0.05$ and periodic boundary conditions. The initial condition is set to the field of ψ having an averaged value of ψ equal to zero, $\langle\psi\rangle = 0$, and a standard deviation from the average value 0.2. We ran our simulations ten times for each set of parameters from different initial configurations and the results were averaged. In this study, the uniaxial compression with compression ratio

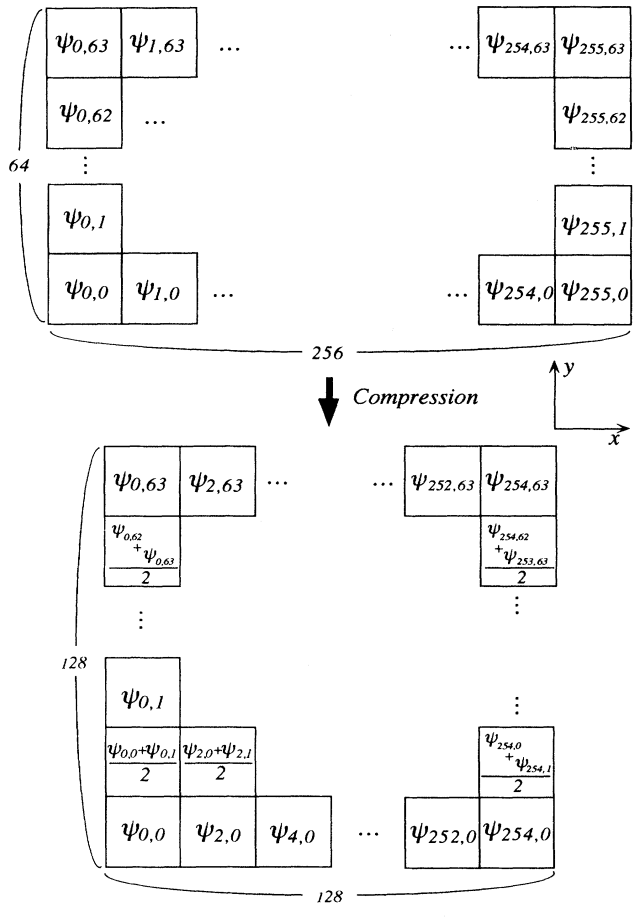

FIG. 3. Schematic diagram showing the method of executing uniaxial compression in computer simulations.

$\gamma_p = \frac{1}{2}$ was simulated as follows on the basis of an affine deformation on the cell size scale. To apply the uniaxial compression *along the x axis* in the xy plane, we deformed 256×64 meshes in x and y axes into 128×128 meshes as shown in Fig. 3. In the y axis or the elongation direction, 64 new cells were added between original cells. The values of each new cell were taken to be the average of two values of the adjacent cells. For the x axis or the compression direction, odd number cells were eliminated. Note that the compression axis taken in the 2D computational study is different from that taken in the experimental system shown in Fig. 2.

We employed three experimental conditions: (i) isothermal SD without compression, (ii) isothermal SD and compression at $t=20$, and (iii) isothermal SD and compression at $t=500$. The time $t=20$ corresponds to the intermediate stage SD [6], where the amplitude of ψ has not yet reached its equilibrium value and both the wavelength and the amplitude of ψ grow with time. On the other hand, the time $t=500$ corresponds to the late stage SD [6], where the amplitude of ψ has reached its equilibrium value and only the characteristic length of ψ grows with time. We investigate the structure factor $S(\mathbf{q},t)$ at time t and at the scattering vector $\mathbf{q} \equiv (q_x, q_y)$, where q_x and q_y are the components of $\mathbf{q}$ parallel and perpendicular, respectively, to the compression axis. We obtain $S(\mathbf{q},t)$ by applying fast Fourier transform to $\langle \psi(\mathbf{r})\psi(0) \rangle$. It is noted that $\mathbf{r}$, t, $\mathbf{q}$, and ψ have no units, since they are reduced variables.

III. RESULTS AND DISCUSSION

A. Isothermal SD process without compression

Figure 4 shows the time change in the phase-separated structure and the profiles of ψ along the horizontal lines

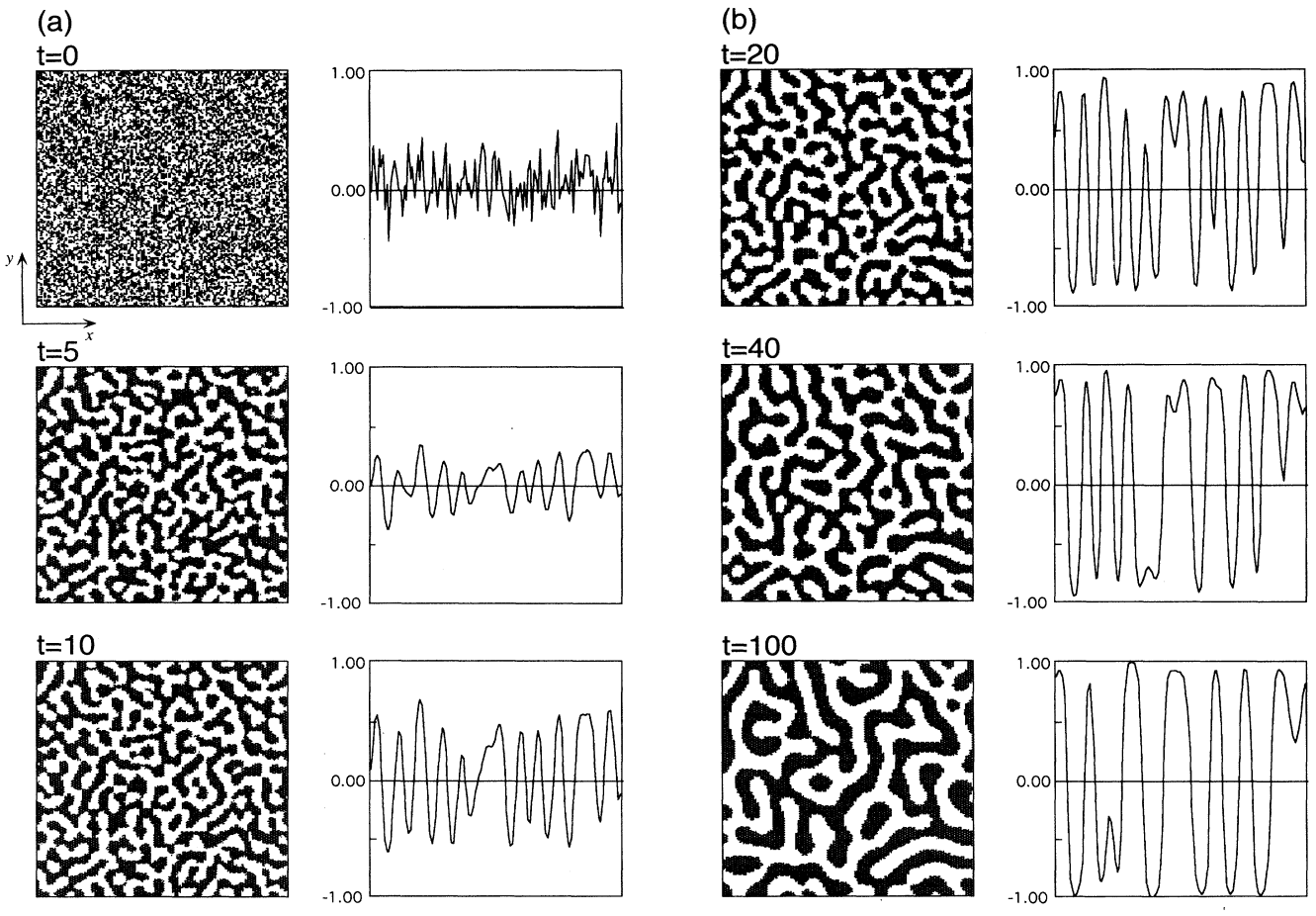

FIG. 4. Time change in the phase-separated structures for the SD processes without compression. The patterns in the left-hand part of the figure are the snapshot pictures of domain structures developed in the systems. Filled and open cells represent A-rich and B-rich cells, respectively. The profiles in the right-hand part of the figure indicate the fluctuations of ψ along the horizontal lines cutting through the centers of the snapshot pictures. The upper and lower limits of the ordinate in the right-hand side of the figure correspond to equilibrium values of ψ.

cutting through the centers in the phase-separated structure during a SD process without compression. Figure 4(a) illustrates the time change of the structure in the early stage SD. The random distribution of ψ changes into a periodic phase-separated structure and the periodic structure keeps its wavelength constant while the amplitude of the structure grows with time. In the intermediate stage SD, the periodic structure coarsens with time and the amplitude of ψ increases with time toward the equilibrium value as shown in Fig. 4(b). The features of the time change in the structure in the late stage SD is that the amplitude of ψ reaches the equilibrium value while the structure coarsens self-similarly with time as shown in Fig. 4(c).

Figure 5 presents time change in the circularly averaged structure factor $S_c(q,t)$ at time t and at q. $S_c(q,t)$ is defined by

$$S_c(q,t)=\frac{1}{2\pi}\int_0^{2\pi} S(\mathbf{q},t)d\mu \ , \tag{7}$$

where μ is the azimuthal angle of $\mathbf{q}$ with respect to the x axis. In the early stage SD, $S_c(q,t)$ increases and decreases with t at $q<1$ and $q>1$, respectively. Here $q_c=\sqrt{c/D}=1$ is the critical wave number of growth. In this stage, the time change in the $\psi_q(t)$ follows Eq. (4), so that $S(q,t)$ is described by

$$S_c(q,t)=S_c(q,0)\exp[2R(q)t] \ , \tag{8}$$

where

$$R(q)=D_{\text{app}}q^2\left[1-\frac{q^2}{2q_m(0)^2}\right] . \tag{9}$$

The quantities D_{app} and $q_m(0)$ are already defined by Eqs. (5) and (6), respectively. It is noted that $q_c^2=2q_m(0)^2$; the characteristic time t_c of our system defined by $t_c=[D_{\text{app}}q_m(0)^2]^{-1}$ is 2. The exponential growth of $S_c(q,t)$ can be seen at $t<10$. The peak of $S_c(q,t)$ first appears around $q=1/\sqrt{2}$ and the peak position does not change with t, as shown in Fig. 5(a), the results of which are consistent with the results predicted by the linearized theory. In the intermediate stage and the late stage SD, however, the peak position then shifts to the smaller q and the peak intensity increases with time, owing to

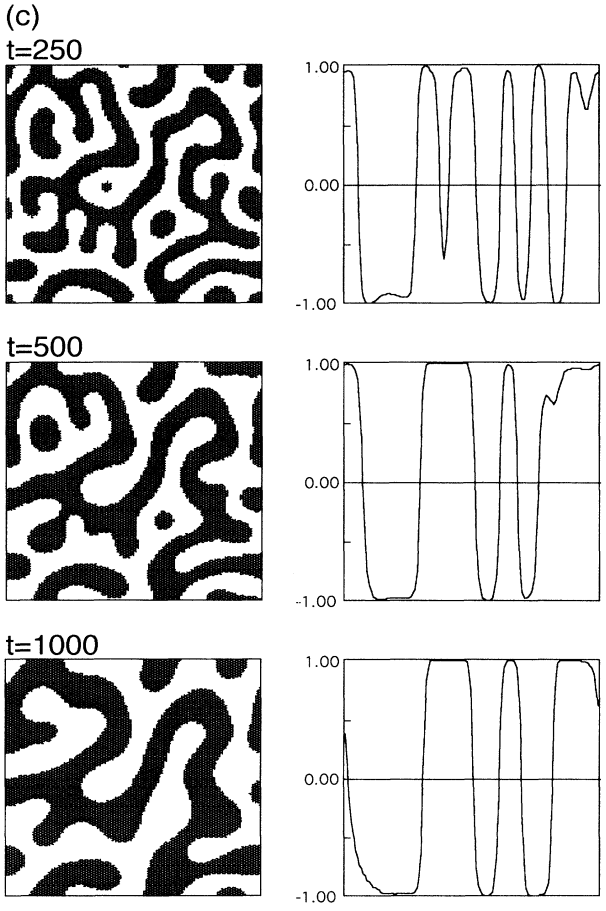

FIG. 4. (*Continued*).

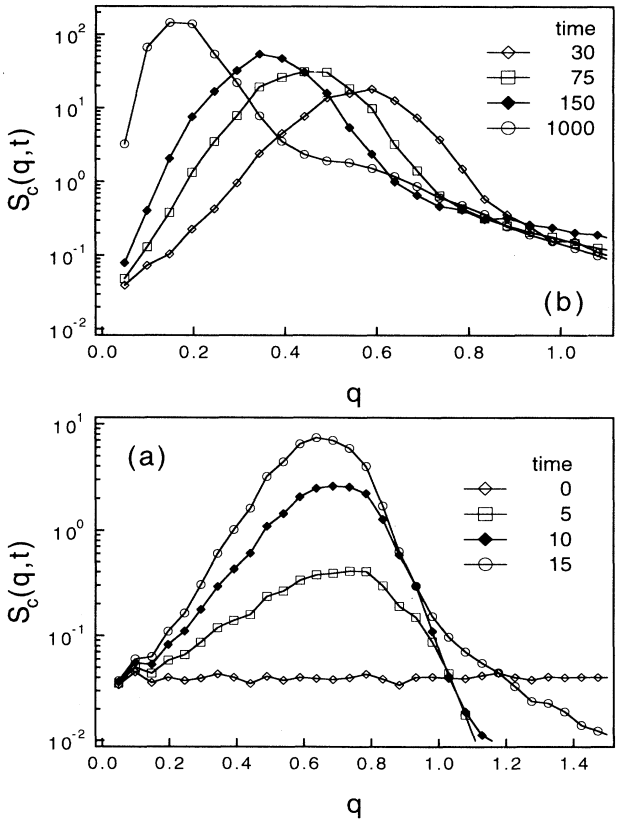

FIG. 5. Time change in the circularly averaged scattered intensity distribution $S_c(q,t)$ during the SD processes without compression.

coarsening of the phase-separated structure as shown in Fig. 5(b).

Figure 6 shows the time change in the first moment of q, $q_1(t)$ in double logarithmic scale. $q_1(t)$ characterizes the characteristic wave number of the phase-separated structure at t and is defined by

$$q_1(t)=\frac{\int_0^\infty qS_c(q,t)dq}{\int_0^\infty S_c(q,t)dq} . \tag{10}$$

The slope of this plot tends to approach $-\frac{1}{3}$ at a long time limit that agrees with the previous results in the case without hydrodynamic interaction [12].

Figure 7 presents the time change in the scaled structure factor $F(x,t)$ defined by

$$F(x,t)\equiv q_1(t)^2 S_c(x,t) , \tag{11}$$

with

$$x\equiv q/q_1(t) . \tag{12}$$

As shown in Fig. 7, $F(x,t)$ at $t<40$ increases with t due to an increase of the amplitude of the concentration fluctuations in the system [Fig. 7(a)], while $F(x,t)$ becomes time independent at $t>40$ [Fig. 7(b)], where the amplitude of the concentration fluctuations reaches the equilibrium value and the $S(q,t)$ can be scaled with the time-dependent characteristic wave number $q_1(t)$. This time $t_{cr}=40$ is the crossover time from the intermediate stage to the late stage. The results indicate that the isothermal SD process without compression can be divided into the three stages: (i) the early stage $0<t<10$, (ii) the intermediate stage $10<t<40$, and (iii) the late stage $40<t$. Hence, compression at $t=20$ and $t=500$ corresponds to those in the intermediate stage and in the late stage, respectively.

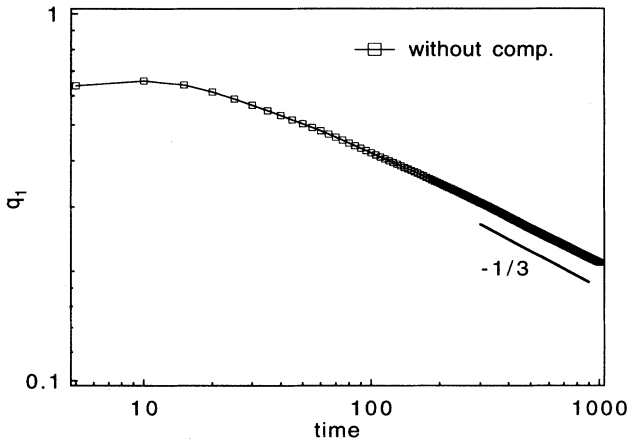

FIG. 6. Time change in q_1 plotted double logarithmically as a function of time t during the SD processes without compression.

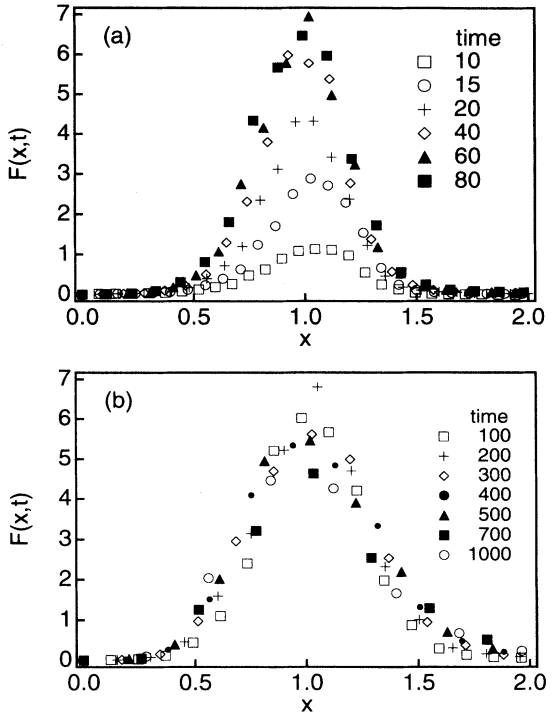

FIG. 7. Time change in the scaled structure factor $F(x,t)$ during the SD processes without compression.

B. Isothermal SD process with a uniaxial compression at $t=20$ (intermediate stage)

The left-hand and the right-hand parts in Fig. 8, show respectively, the time change in the phase-separated structure and the profile of ψ along the horizontal lines cutting through the centers during a SD process before [part (a)] and after [parts (b) and (c)] compression at $t=20$. Before the compression is applied to the system, the random distribution of ψ changes into an isotropic periodic phase-separated structure, as shown in the left-hand parts in Fig. 8(a). The fluctuation profiles from $t=0$–15 indicate that the fluctuations did not reach their equilibrium values before the compression. The pattern and the fluctuation profile at $t=20$ in Fig. 8(b) displays those just after compression. The compression direction is horizontal as indicated by the arrow in the figure. The compression makes the pattern elongated and oriented in the direction perpendicular to the compression axis, i.e., the interfaces of the domains tend to orient parallel to the y axis. The compression ratio of $\frac{1}{2}$ applied at the intermediate stage SD (at $t=20$) is found to have interesting effects on further growth of the pattern with time as shown in Figs. 8(b) and 8(c). Surprisingly, the orientation direction of the pattern appears to change from the direction perpendicular to the direction parallel to the compression axis as time after the compression increases, i.e., the domains with their interfaces parallel to y axis disappear and those with their interfaces parallel to the x

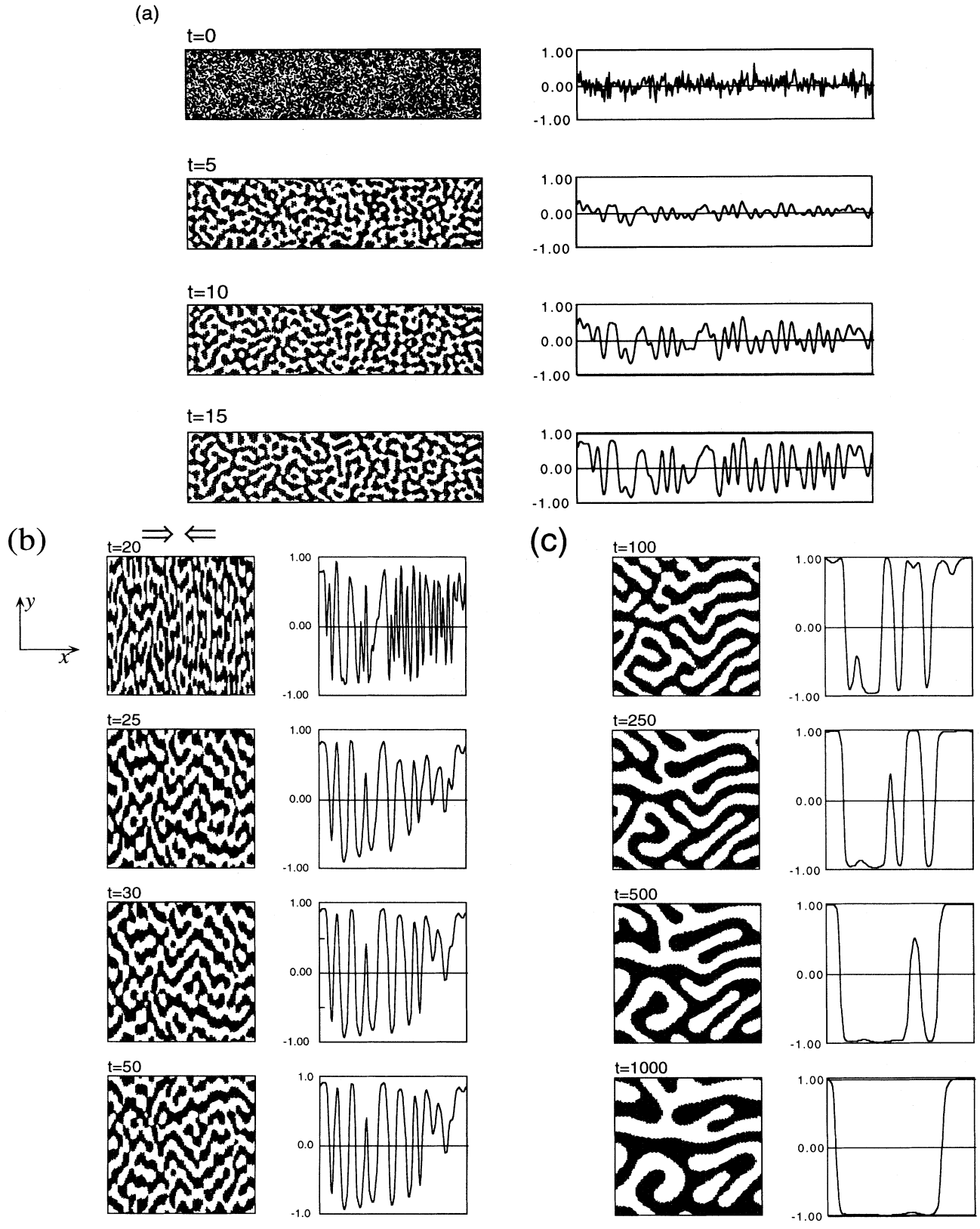

FIG. 8. Time change in the phase-separated structures during the SD processes before (a) and after (b) compression at $t=20$. The meaning of the figure is the same as that of Fig. 4. Arrows above the snapshot at $t=20$ indicate the compression axis.

axis become influential.

This interesting result is shown more clearly by the time change in $S(\mathbf{q},t)$ in two dimensions. Figure 9 shows the time change in $S(\mathbf{q},t)$ after compression, where q_x and q_y are the components of $\mathbf{q}$ parallel and perpendicular to the compression direction, respectively. At $t=20$, a trajectory $\mathbf{q}$ giving rise to a maximum intensity in $S(\mathbf{q},t)$ is elongated in the compression direction, reflecting the phase-separated structure elongated along the direction perpendicular to the compression axis. It should be noted that the peak intensity along the q_x and q_y directions has almost the same value just after compression at $t=20$. However, $S(\mathbf{q},t)$ around the q_x axis decreases with time during the coarsening after

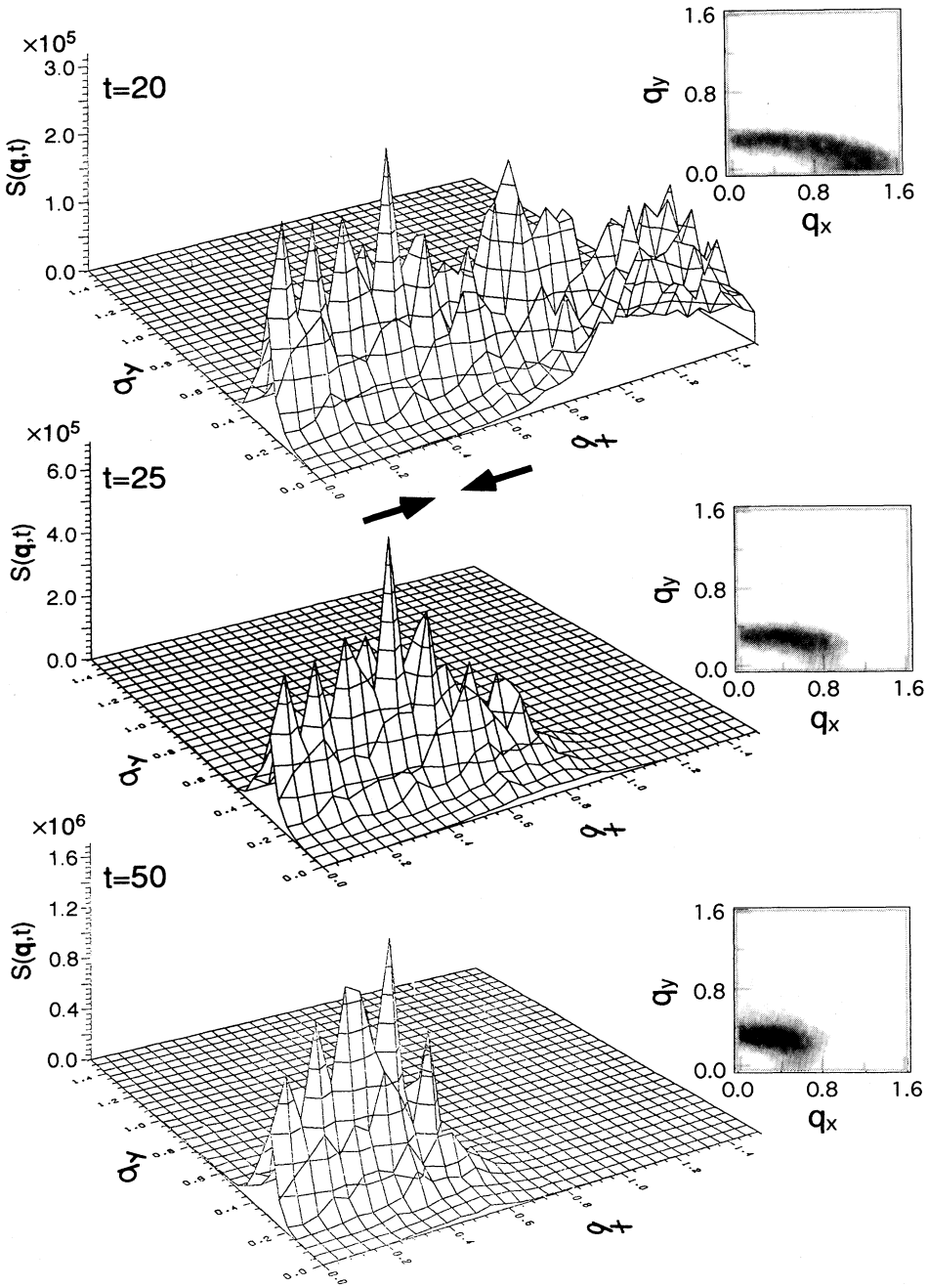

FIG. 9. Time change in $S(\mathbf{q},t)$ plotted as a function of scattering vectors $\mathbf{q}$ during SD processes and after compression at $t=20$, where q_x is a component of $\mathbf{q}$ parallel to the compression axis. The left-hand part of the figure is the bird's view of $S(\mathbf{q},t)$. The right-hand part of the figure is the density plot of the $S(\mathbf{q},t)$ corresponding to the left-hand part.

compression, while that around the q_y axis increases as time elapses. At $t=100$, the main parts of $S(\mathbf{q},t)$ are biased along the q_y axis, so that the scattering pattern appears to show a two-point pattern oriented along q_y. This indicates that the domains that develop are oriented with their interfaces parallel to the x axis, i.e., the compression axis. In the time domain from $t=100$–1000, a new peak appears along the x axis, the peak position shifts toward smaller q, and the peak intensity increases with time. On the other hand, the peak position along the y axis changes negligibly with time and only the peak intensity increases with time.

In order to explore the reason why the orientation direction changes with time during the coarsening process after compression, we focus on the time changes in intensity of the $S(\mathbf{q},t)$ along the q_x axis, $S_x(q,t)\equiv S(q_x,q_y=0,t)$, and along the q_y axis, $S_y(q,t)\equiv S(q_x=0,q_y,t)$. Figure 10 shows the time change in $S_x(q,t)$ before [part (a)] and after [part (b)] compression. The compression shifts the peak position from $q\cong 0.6$ to $q\cong 1.2$ for $S_x(q,t)$. The shifted peak then loses intensity with time at t slightly longer than

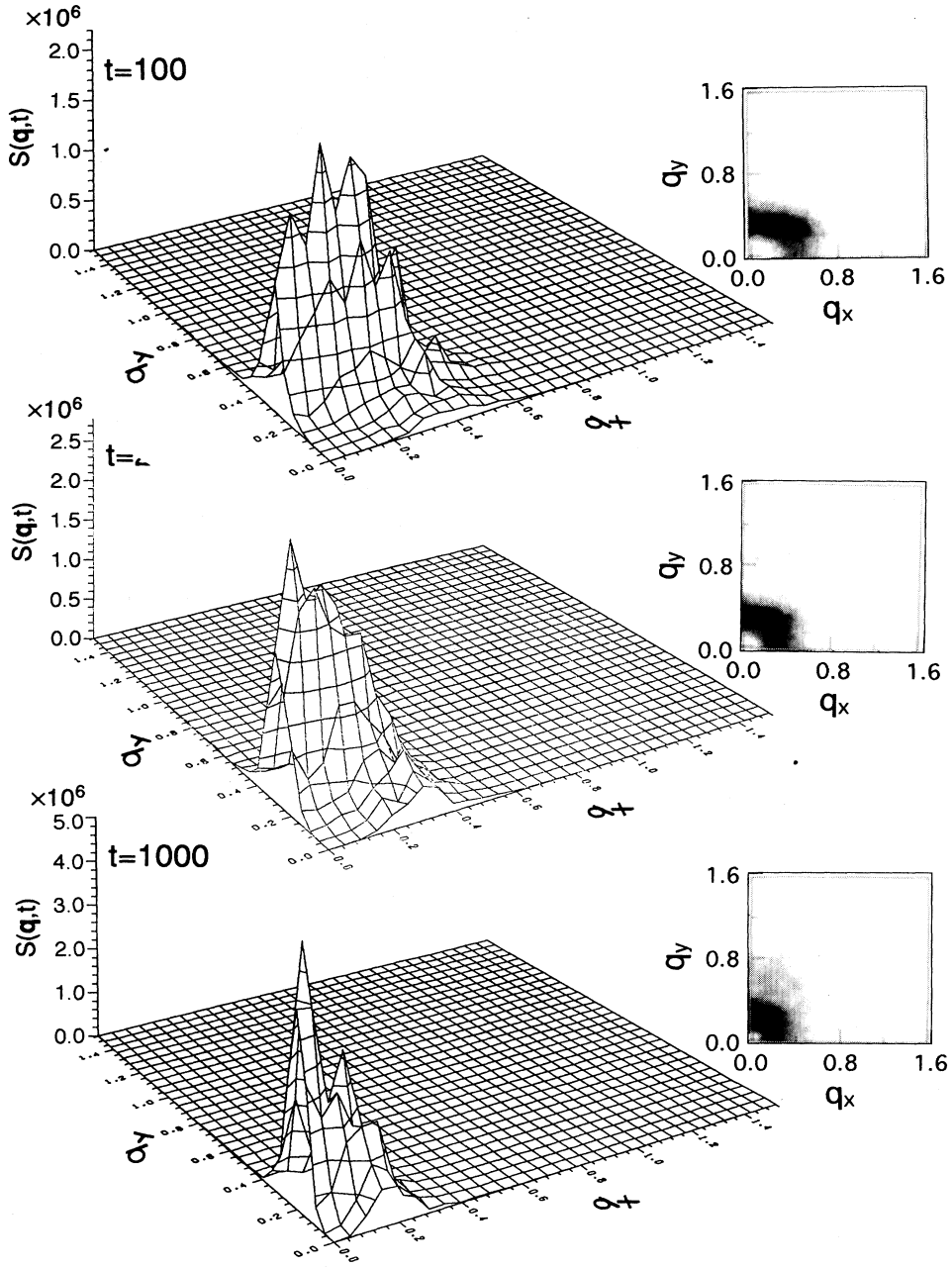

FIG. 9. (*Continued*).

$t=25$. The reason for the reduction of $S_x(q,t)$ upon compression is the shift of the $q_m(t)$ for the dominant mode of the concentration fluctuations beyond q_c so that the fluctuations for $q>q_c$ decay even after the early stage SD [8].

After the disappearance of the peak of $S_x(q,t)$ around $q=1.2$ (see the profile at $t=20$), a new peak appears at $q=0.8$ (see the profile at $t=25$) and the peak shifts to smaller q while the peak intensity increases with time, as expected for the usual coarsening process. The behavior of $S_x(q,t)$ indicates that the ordering processes via SD restarts and that the fluctuations of the order parameters grows after the disappearance of the original peak.

On the other hand, as shown in Fig. 11, the compression shifts the peak position of $S_y(q,t)$ from $q\cong 0.6$ to $q\cong 0.3$, which reflects the fact that the domain structure is elongated along the y axis. After compression, the peak position of $S_y(q,t)$ is kept constant from $t=20$ to 250, as found in the experiments [5]. Then the peak shifts toward smaller q while the peak intensity increases as seen in the profiles obtained from $t=250$ to 1000. This result agrees with the experimental result reported by Hashimoto and Izumitani [5]. The increases of the peak intensity means that the characteristic length of the phase-separated structure and the amplitude of the concentration fluctuations grow with time.

A comparison between $S_x(q,t)$ and $S_y(q,t)$ at $t=1000$ indicates that the peak intensity of $S_y(q,t)$ is about 5 times larger than that of $S_x(q,t)$. This reflects the compression effect: the concentration fluctuations in the

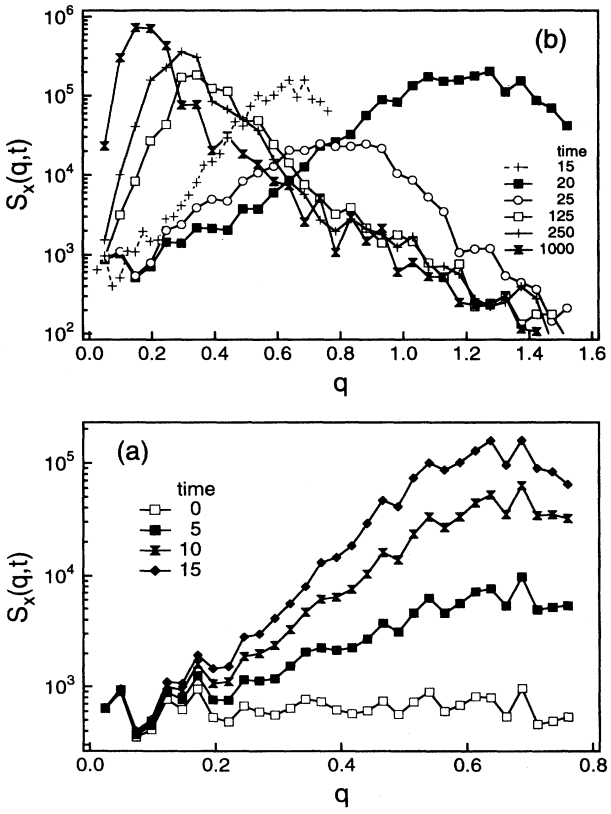

FIG. 10. Time change in $S_x(q,t)$ during SD processes before (a) and after (b) the compression at $t=20$.

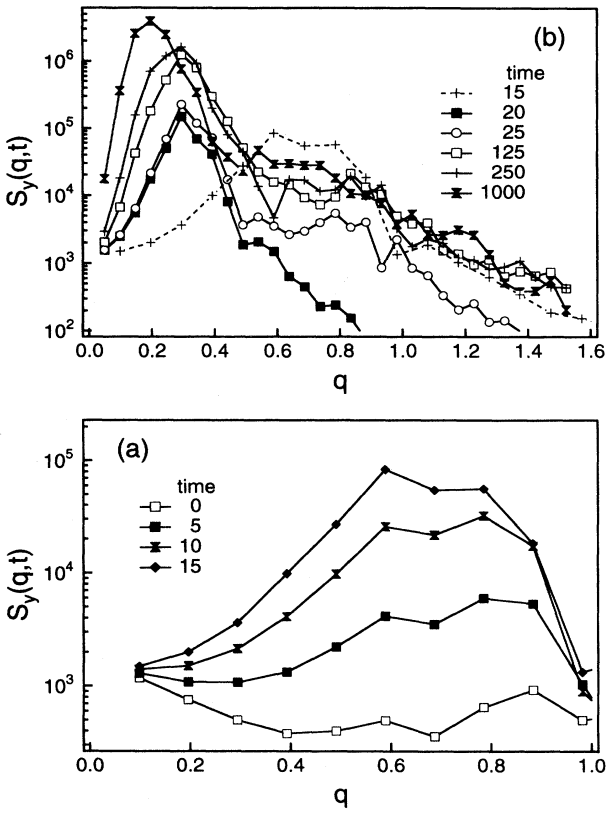

FIG. 11. Time change in $S_y(q,t)$ during SD processes before (a) and after (b) compression at $t=20$.

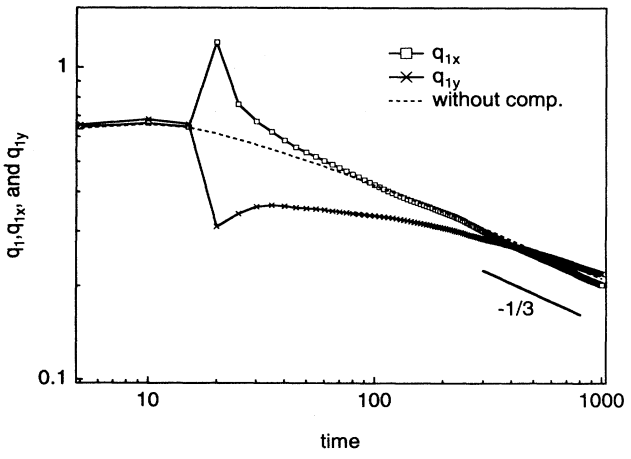

FIG. 12. Time changes in q_1, q_{1x}, and q_{1y} plotted double logarithmically as a function of t. q_1, q_{1x}, and q_{1y} are defined by Eqs. (10), (13), and (14), respectively.

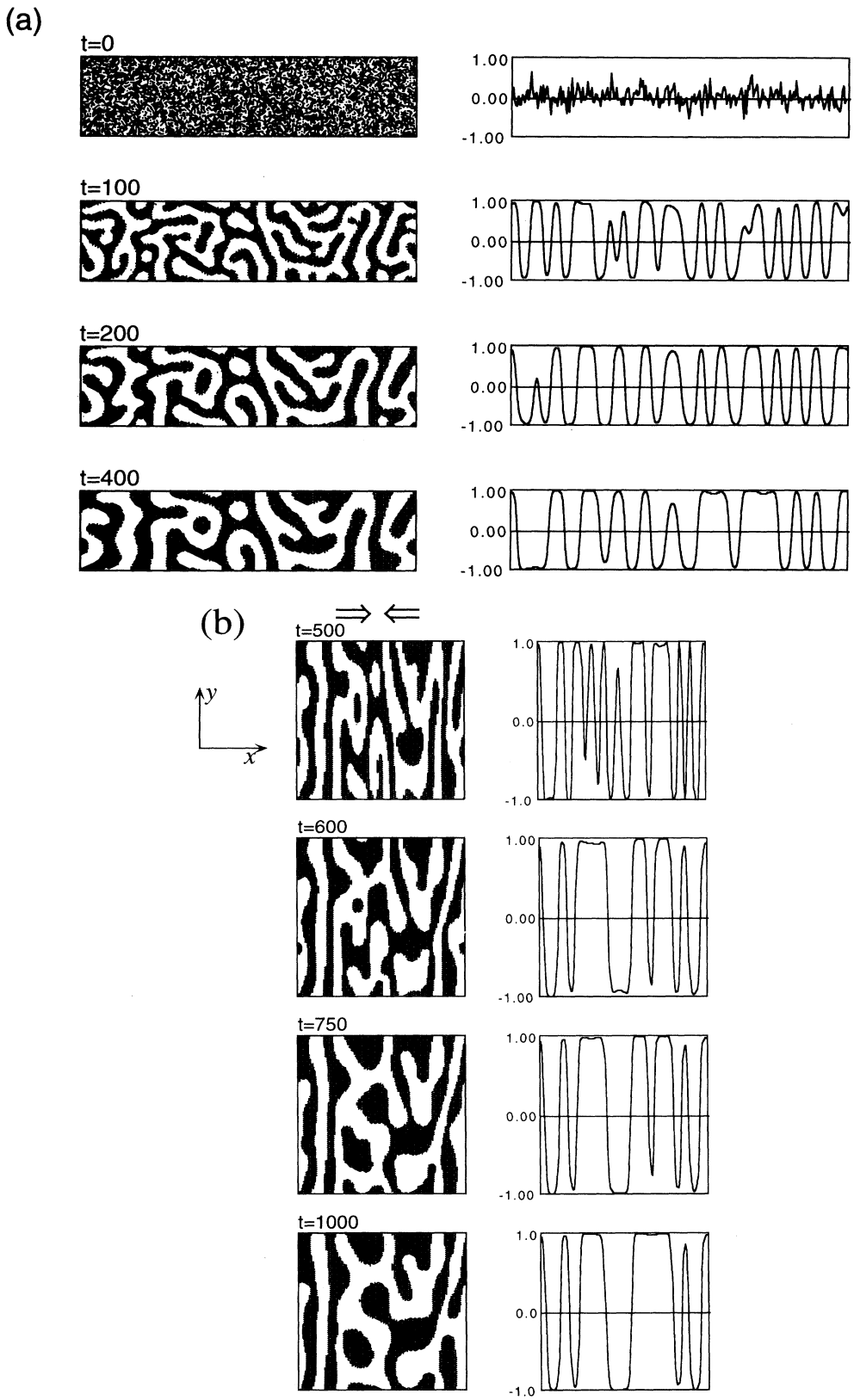

FIG. 13. Time change in the phase-separated structures during the SD processes before (a) and (b) and after the compression at $t=500$. The meaning of the figure is the same as that of Fig. 4. Arrows above the snapshot at $t=500$ indicates the compression axis.

compression axis disappear at $t=20$, while those in the y direction do not. The compression effect gives rise to a unique orientation of the domain structure with interfaces parallel to the compression axis.

Figure 12 shows the time change in the characteristic wave number q_{1x} and q_{1y} parallel and perpendicular to the compression axis, respectively, in double logarithmic scale. Here q_{1x} and q_{1y} are defined by

$$q_{1x}(t)=\frac{\int_0^\infty qS_x(q,t)dq}{\int_0^\infty S_x(q,t)dq} \tag{13}$$

and

$$q_{1y}(t)=\frac{\int_0^\infty qS_y(q,t)dq}{\int_0^\infty S_y(q,t)dq} . \tag{14}$$

In Fig. 12, the broken line corresponds to the time change in q_1 for the SD process without compression as already shown in Fig. 6. The characteristic wave number q_{1x} shifts to the higher q after compression and then the time change in q_{1x} gradually approaches that of the case without compression. The slope of the plot at a long time limit is $-\frac{1}{3}$ in agreement with the results [12] without hydrodynamic interactions, which indicates that the ordering processes via SD restarts after compression. On the

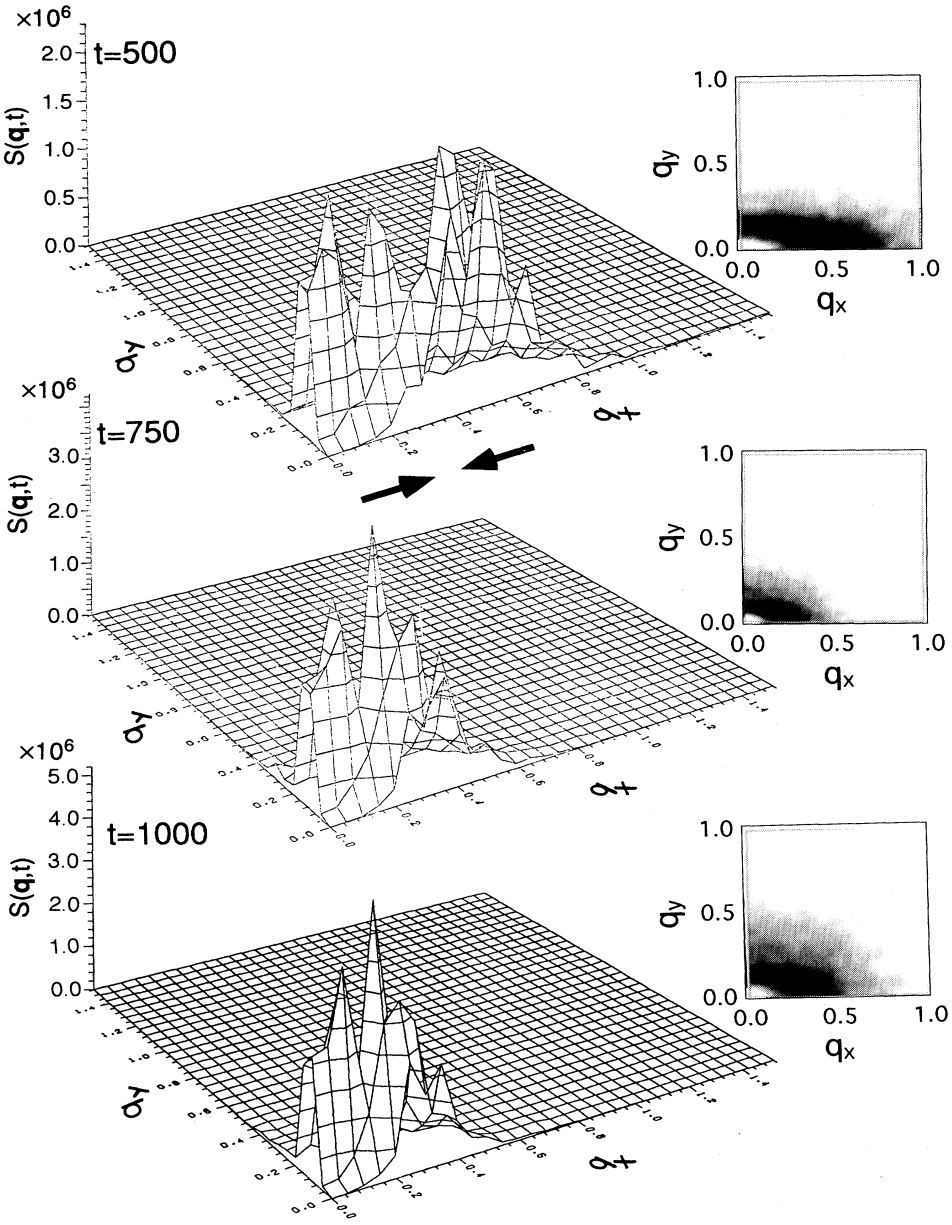

FIG. 14. Time change in $S(\mathbf{q},t)$ distribution plotted as a function of scattering vectors $\mathbf{q}$ during the SD processes after compression at $t=500$. The meaning of the figure is the same as that of Fig. 9.

other hand, q_{1y} first shifts to the lower q by compression, then is kept almost constant with time after compression from $t=30$ to $t=100$, and finally the time change in q_{1y} approaches that in q_1 without compression. The results are consistent with the experimental one [5]. The relaxation of the compression effect is due to the nonlinear effect associated with the term $u\psi^3$ in Eq. (2). It is interesting to note the anisotropy in the relaxation process: the relaxation parallel to the compression axis is much faster than that perpendicular to it. This anisotropy can be understood because the modes having higher q have a stronger thermodynamic driving force for decay than those having lower q and hence the former relaxes faster than the latter. A small mismatch among q_{1x}, q_{1y}, and q_1 at the long time limit of our study is within the experimental errors of our computational accuracy.

C. Isothermal SD process with a uniaxial compression with compression ratio $\frac{1}{2}$ at $t=500$ (late stage)

The left- and the right-hand parts of Fig. 13 show the time change in the phase-separated structure and the profile of ψ along the horizontal lines cutting through the centers in the left-hand parts, respectively, during the SD process before [part (a)] and after [part (b)] the compression at $t=500$. Before compression is applied, the random distribution of ψ changes into a periodic phase-separated structure and the structure coarsens with time as shown in the patterns from $t=0$–400. These structures are isotropic. The fluctuation profiles at $t=400$ indicate that the amplitudes of concentration fluctuations

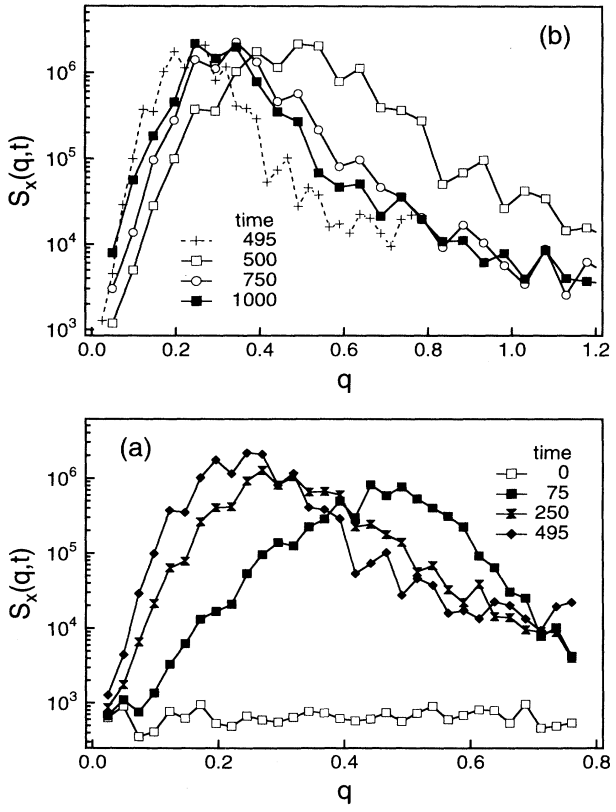

FIG. 15. Time change in $S_x(q,t)$ during the SD processes before (a) and after (b) compression at $t=500$.

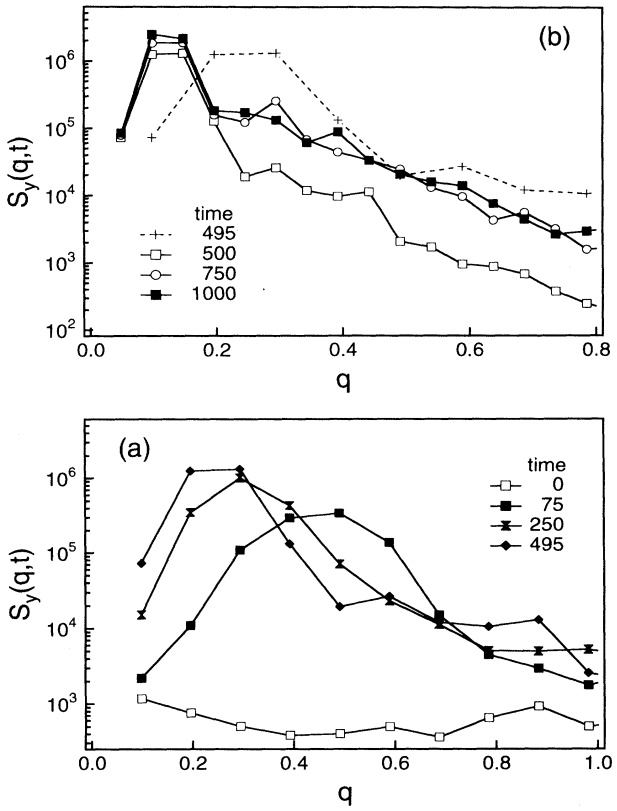

FIG. 16. Time change in $S_y(q,t)$ during the SD processes before (a) and after (b) compression at $t=500$.

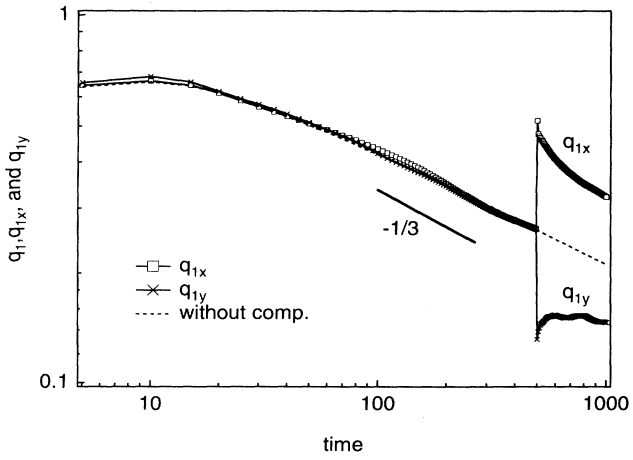

FIG. 17. Time changes in q_1, q_{1x}, and q_{1y} plotted double logarithmically as a function of t. q_1, q_{1x}, and q_{1y} are defined by Eqs. (10), (13), and (14), respectively.

before compression have already reached their equilibrium values, which is different from the case with compression at $t=20$. The pattern and the fluctuation profile at $t=500$ show those just after compression. The compression direction is indicated by an arrow in the figure. The compression makes the pattern elongated and oriented with interfaces parallel to the y axis, as in the case with compression at $t=20$. After compression, the structure coarsens with time, while keeping the orientation direction of the interfaces essentially unchanged. Therefore, the result is very different from the case with the compression at $t=20$.

Figure 14 shows the time change in $S(\mathbf{q},t)$ after compression in two dimensions. The peak intensity in each direction increases with time, which is different from the behavior in the case with the compression at $t=20$. Figures 15 and 16 show the time changes in $S_x(q,t)$ and $S_y(q,t)$ before [part (a)] and after [part (b)] compression at $t=500$, respectively. Contrary to the results for the case with compression at $t=20$, the reduction of $S_x(q,t)$ after compression does not occur but the peak position of $S_x(q,t)$ shifts toward larger q while the peak intensity of $S_x(q,t)$ is kept almost constant [see Fig. 15(b)]. The behavior of $S_y(q,t)$ after compression at $t=500$ [Fig. 16(b)] is similar to that in the case with compression at $t=20$: the peak position of $S_y(q,t)$ keeps almost constant and the peak intensity of $S_y(q,t)$ increases with time. At $t=1000$, the peak intensity of $S_x(q,t)$ is almost as large as that of $S_y(q,t)$. This indicates that the structure is only elongated and that the amplitude of the concentration fluctuations is not affected by compression.

Figure 17 shows time changes in q_{1x} and q_{1y} for the case with compression at $t=500$. Here again the broken line shows the behavior of q_1 without compression. After compression, q_{1x} decreases rapidly with time between $t=500$ and 800 and then tends to gradually approach the level of q_1 without compression. On the other hand, q_{1y} rapidly increases with time between $t=500$ and 600 and then is kept constant with time from $t=600$ to 1000.

The difference between the pattern developed after compression at $t=20$ and that at $t=500$ comes from a difference in the stability of the Fourier modes of the concentration fluctuations in the q_x axis after compression. In the case of compression at $t=20$, the modes will decay, since their q are shifted to the values larger than q_c. On the other hand, in the case of compression at $t=500$, the domain structures are well developed, characterized by a considerably large domain size, equilibrium local compositions, and well defined interface. Hence, most of the Fourier modes have their wave numbers smaller than q_c, before and after compression. Although they are deformed with compression, they do not decay. The concentration fluctuations further grow with time after deformation to result in the coarsening and the formation of the unique domain structure.

IV. CONCLUSION

Effects of uniaxial compression on ordering processes via SD in binary mixtures were investigated by computer simulations based on the TDGL equation. The scattered intensity distribution in two-dimensional space shows that the compression in the intermediate stage SD causes the phase-separated structure to be oriented with their interfaces parallel to the compression axis. The origin of the unique orientation of the domain structure is found to be attributed to the fact that the most of the q modes of the concentration fluctuations with their wave vectors along the compression axis decay after compression, but the q modes with their wave vectors perpendicular to the compression axis do not decay, although they are deformed into longer wavelengths. Further growth of the domains continues even after compression in the context of the TDGL equation subjected to the new initial condition produced by uniaxial compression. The unique initial condition results in the unique domain structure. The reason the decay of the modes occurs is that they have wave numbers larger than the critical wave number q_c after compression. The decay of the Fourier modes of the concentration fluctuations induced by compression can support our proposed homogenization mechanism brought by Baker's transformation [4], i.e., a binary mixture containing phase-separated structure can be brought into a single-phase mixture near the point on the binodal curve when it is subjected to a repeated uniaxial compression. Thus the present computational study can give supporting evidence for our hypothesis on *the homogenization induced by Baker's transformation.* On the other hand, compression in the late stage SD causes the phase-separated structure to be oriented in the direction perpendicular to the compression axis, because the domain structures are already well developed and compression in the late stage SD does not lead to the decay of the modes. This is because even after compression q_{1x} is still smaller than q_c. However, if compression is repeatedly applied to the system, most of the modes are compressed so that their wave numbers eventually become greater than q_c, resulting in the decay discussed above. Hence the mixtures should be brought into a single phase, providing a theoretical interpretation for the homogenization induced by Baker's transformation.

ACKNOWLEDGMENTS

M.T. and T.H. express their thanks to Mr. Tatsuo Izumitani and Dr. Tuyoshi Koga for useful discussions. Part of this work was supported by grant-in-aid for encouragement of young scientists A (02953046) and a grant-in-aid for scientific research (05453149) from the Ministry of Education, Science and Culture of Japan.

[1] J. D. Gunton, M. San Miguel, and P. S. Sahni, in *Phase Transition and Critical Phenomena,* edited by C. Domb and J. L. Lebowitz (Academic, New York, 1983), Vol. 8, Chap. 3, p. 269; K. Binder, in *Materials Science and Technology,* edited by R. W. Cahn, P. Haasen, and E. J. Kramer (VCH, Weinheim, 1991), Vol. 5, Chap. 7, p. 405; T. Hashimoto, in *Materials Science and Technology,* edited by R. W. Cahn, P. Haasen, and E. J. Kramer (VCH, Weinheim, 1993), Vol. 12, Chap. 6, p. 251.

[2] E. Helfand and G. H. Fredrickson, Phys. Rev. Lett **62**, 2468 (1989); A. Onuki, *ibid.* **62**, 2472 (1989); J. Phys. Soc. Jpn. **59**, 3424 (1990); M. Doi and A. Onuki, J. Phys. II (France) **2**, 1631 (1992).

[3] G. Ver Strate and W. Phillipoff, J. Polymer. Sci. Polymer. Lett. **12**, 267 (1974); C. Rangel-Nafaile, A. B. Metzner, and K. F. Wissburn, Macromolecules **17**, 1187 (1984); T. Hashimoto, T. Takebe, and S. Suehiro, J. Chem. Phys. **88**, 5874 (1988); T. Takebe, R. Sawaoka, and T. Hashimoto, J. Chem. Phys. **91**, 4369 (1989); T. Hashimoto and K. Fujioka, J. Phys. Soc. Jpn. **60**, 365 (1991); X. L. Wu, D. J. Pine, and P. K. Dixon, Phys. Rev. Lett **66**, 2408 (1991); J. W. van Egmond, D. E. Werner, and G. Fuller, J. Chem. Phys. **96**, 7742 (1992); T. Hashimoto, T. Takebe, and K. Asakawa, Physica A **194**, 338 (1993); E. Moses, T. Kume, and T. Hashimoto, Phys. Rev. Lett **72**, 2037 (1994).

[4] T. Hashimoto, T. Izumitani, and M. Takenaka, Macromolecules **22**, 2293 (1989).

[5] T. Hashimoto and T. Izumitani, Polym. Prepr. Am. Chem. Soc. Div. Polym. Chem. **26**, 66 (1985); T. Izumitani and T. Hashimoto (unpublished).

[6] T. Hashimoto, Phase Transitions **12**, 47 (1988).

[7] T. Izumitani and T. Hashimoto, J. Chem. Phys. **83**, 3694 (1985); M. Takenaka, T. Izumitani, and T. Hashimoto, Macomolecules **20**, 2257 (1987); T. Izumitani, M. Takenaka, and T. Hashimoto, J. Chem. Phys. **92**, 3213 (1990); M. Takenaka, T. Izumitani, and T. Hashimoto, J. Chem. Phys. **92**, 4566 (1990).

[8] J. W. Cahn, J. Chem. Phys. **42**, 93 (1965).

[9] K. Kawasaki, Physica **119A**, 17 (1983).

[10] H. E. Cook, Acta. Metall. **18**, 297 (1970).

[11] K. Kawasaki, Prog. Theor. Phys. **57**, 826 (1977).

[12] Y. Oono and S. Puri, Phys. Rev. A **38**, 434 (1988); S. Puri and Y. Oono, Phys. Rev. A **38**, 1542 (1988); A. Chakrabarti and J. D. Gunton, Phys. Rev. B **37**, 3798 (1988).

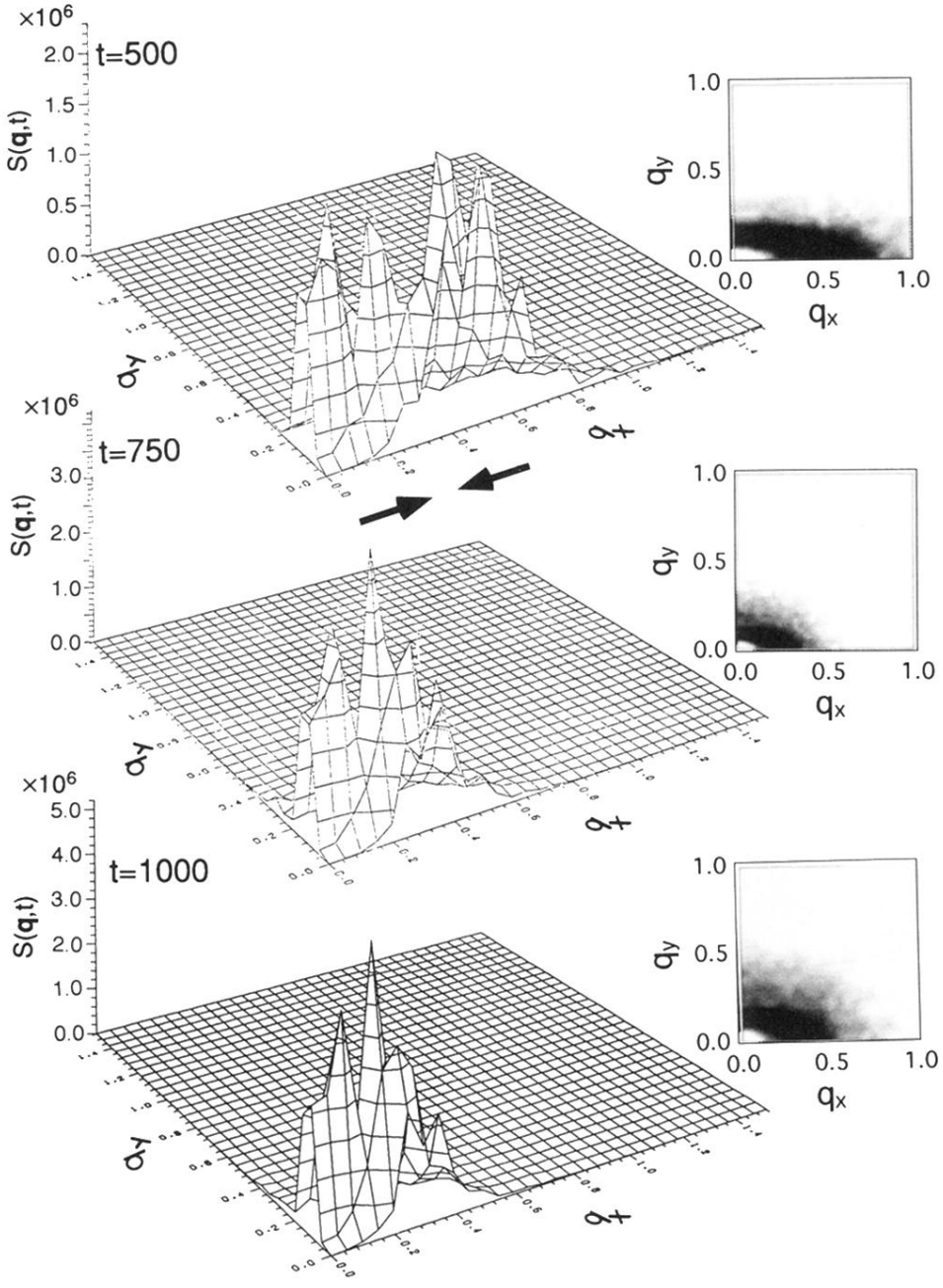

FIG. 14. Time change in $S(\mathbf{q},t)$ distribution plotted as a function of scattering vectors $\mathbf{q}$ during the SD processes after compression at $t=500$. The meaning of the figure is the same as that of Fig. 9.

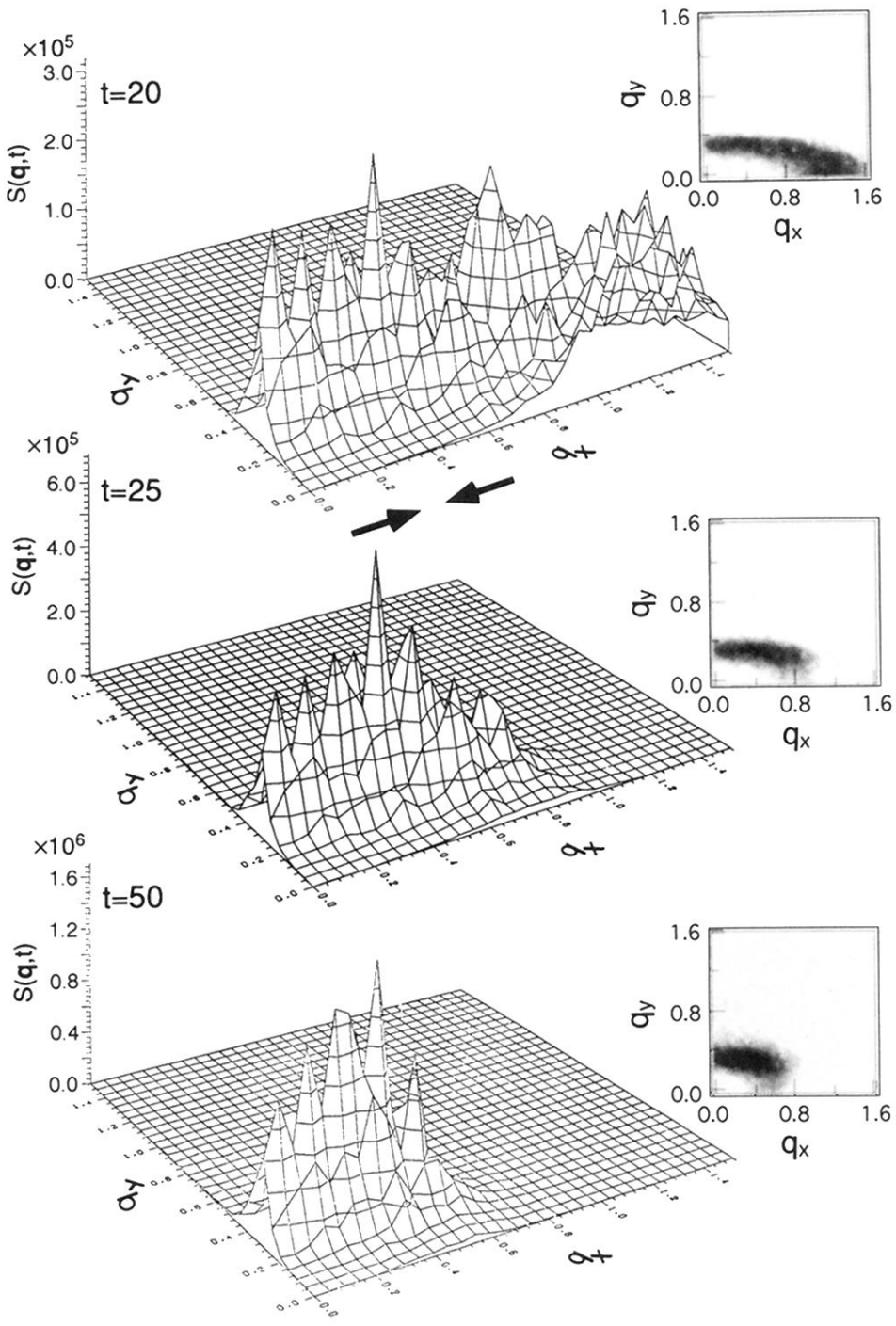

FIG. 9. Time change in $S(\mathbf{q},t)$ plotted as a function of scattering vectors $\mathbf{q}$ during SD processes and after compression at $t=20$, where q_x is a component of $\mathbf{q}$ parallel to the compression axis. The left-hand part of the figure is the bird's view of $S(\mathbf{q},t)$. The right-hand part of the figure is the density plot of the $S(\mathbf{q},t)$ corresponding to the left-hand part.

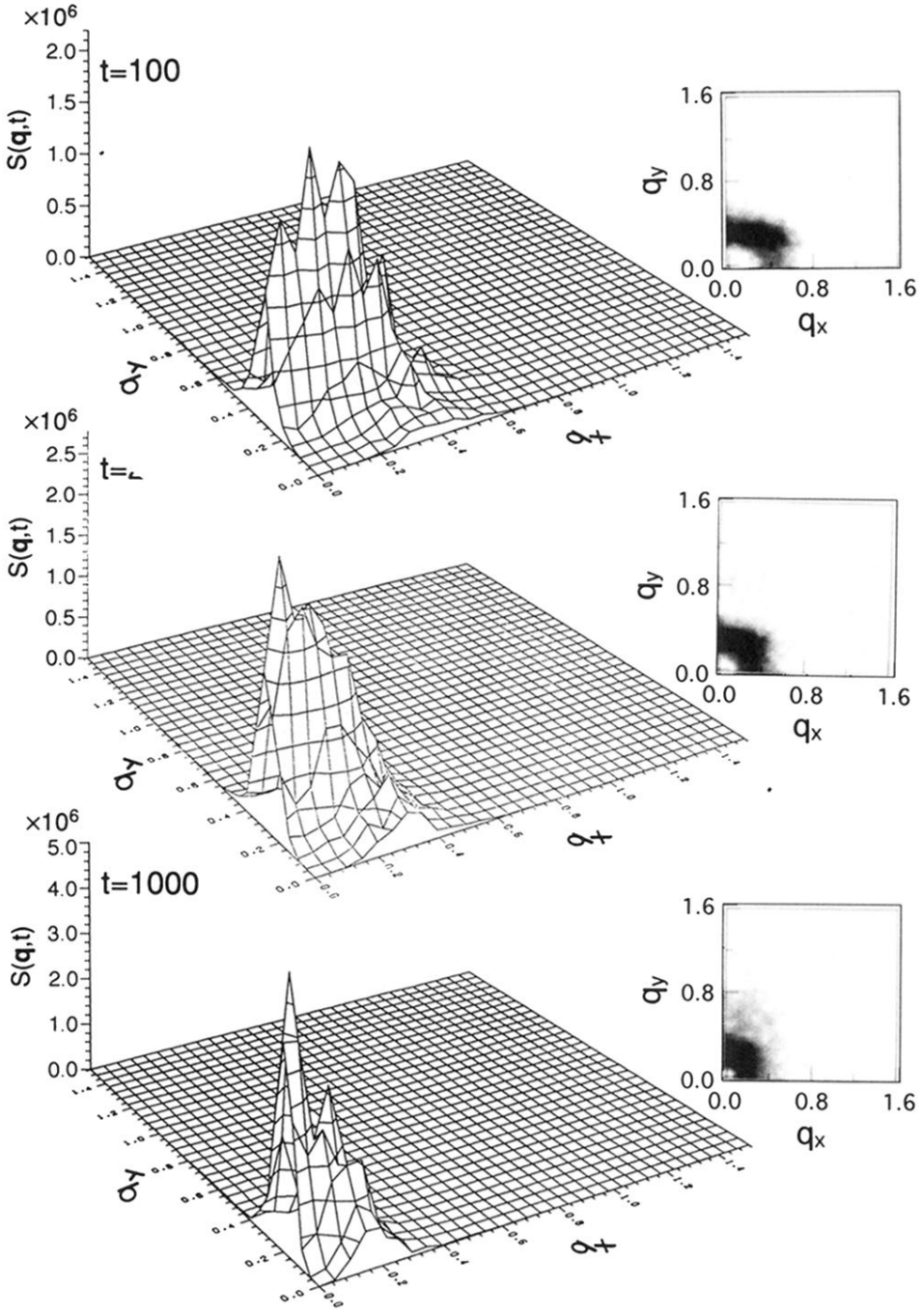

FIG. 9. (*Continued*).